Research Article

A facile method for synthesis rGO/Ag nanocomposite and its uses for enhancing photocatalytic degradation of Congo red dye

Mohamed H. H. Ali[1] · Mohamed E. Goher[1] · Afify D. G. Al-Afify[1] · Siliem M. El-Sayed[1]

Abstract

The enhancing breakdown of dyes using facile, novel and eco-friendly photocatalyst without remaining any hazards secondary intermediates from the dye species regarded one of the most challenges to the healthy world. A novel facile method was used to synthesize reduced graphene oxide (rGO) with various doping ratios of silver nanoparticles (Ag NPs) and applied as photocatalyst to enhancing removal of Congo red (CR) dye using UV light irradiation from aqueous solution. Some characterization features such as UV-diffuse reflectance spectra, TEM, SEM, FTIR, X-ray diffraction, and EDX were measured to demonstrate the energy gap, morphology, size distribution, crystalline nature, phase structure, and elemental compositions of as-synthesized nanoparticles. The effect of some important factors such as pH of solution, initial CR concertation (Co), amount of rGO@Ag (g) and contact time (t) were studied to detect the optimum adsorption condition. The results indicated that, the maximum CR dye photodegradation is obtained at pH 7, 120 min, 50 mg/L initial CR concentration and 0.4 g/L photocatalyst dosage. The photodegradation data declared that, the higher the Ag doping ratio, the higher the degrading efficiency. Isotherm and kinetic studies showed that Langmuir and Freundlich models and the pseudo-second-order model are well fitting the adsorption process with maximum CR adsorption values ranging between 86.95 and 98.04 mg/L with corresponding $R^2 > 0.99$.

Article Highlights

1. A cheap eco-friendly and facile method to synthesis rGO@Ag NPs
2. photodegradation of Congo red dye using as-synthesized rGO@Ag NPs under UV irradiation light
3. a promising photodegradation process of CR dye from aqueous solution was achieved

1 Introduction

In the past few decades, industrial activities have been propagated, especially in developing countries, the industrial wastewaters pose great health risk problems due to their organic and inorganic pollutants [1]. A massive using of the organic dyes in the paper and textiles industries may cause a serious environmentally problems. More than 10,000 different pigments and dyes are used annually in the world [2, 3]. Using synthetic-hued dyes in numerous sectors, including textile, paper and pulp, cosmetics, and leather, results in a rise of colored organic dyes in the trash [4, 5]. A significant

✉ Mohamed E. Goher, smgoher@yahoo.com; Mohamed H. H. Ali, mhha_ali@yahoo.com; Afify D. G. Al-Afify, afifydardeir@yahoo.com; Siliem M. El-Sayed, seliemdabour@gmail.com | [1]National Institute of Oceanography and Fisheries (NIOF), Cairo, Egypt.

quantity of dyes (1%–10%) was wasted in the product dying process, and these amounts were drained with effluents; the dye tailings are highly carcinogenic chemicals [6].

Congo red (CR) dye is widely used in textiles, paper, cosmetics, chemicals, and pharmaceutical industries [7]. Because of its intensive use, a considerable amount of CR residuals is discovered in wastewater that reaches surface water. Because of the remarkable stability of CR dye in light, water, and detergents poses a severe risk to humans and aquatic species [8, 9].

The adsorption process has been possessed a great advantage: it completely removes -in much cases- the dyes molecules without hazard intermediate [10]. Moreover, the recycling possibilities of the adsorbed dye from the residue after the adsorption process thus it would be considered economically and eco-friendly approaches for wastewater treatment [11, 12]. Applicability and efficiencies of the adsorption process mainly depend on the adsorbent capacity and economically cost of the technology [13].

In the last decades, several studies have been carried out to eliminate the organic compounds from wastewater e.g., chemical, physical, and biological methods [14]. However, some classic technologies have several drawbacks, including a poor degrading impact of organic chemicals, large costs, and difficult procedures [15]. As a result, it has become critical to create and develop more sensitive, effective, less costly, eco-friendly, and adaptable technologies for removing and degrading organic contaminants. Consequently, nanomaterials have become efficient techniques for degrading dyes and organic pollutants from aqueous solutions, CeO_2-PPy-ZnO [16]; polyaniline (PAni) and PAni/starch composites [12], para-aminobenzoic acid modified activated carbon [17], mesoporous TiO_2/ZSM-5 [10], ceria NPs [7], NiO NPs [9], Fe_2O_3-CeO_2 nanocomposite [18], alginate/carboxymethyl cellulose/TiO_2 nanocomposite [19], NiS NPs [6], and ZnO NPs [5, 20].

Silver NPs have attracted many researchers; hence, they are regarded as widely and important nanoparticles in nanotechnology processes. Its distinct physicochemical properties make it widely used in various industries, including agriculture, health, medicine, home appliances, packaging, and electronics [21]. 2D graphene sheets have been widely employed because of their larger surface area, excellent physical and chemical properties, and ability to control their properties through chemical functionalization. The reduction of GO to synthesize the reduced graphene oxide (rGO) is widely used nowadays to improve and support the Nano catalyst's features [22]. Furthermore, among the numerous forms of NPs, magnetic particles have been widely used in nanocatalyst production due to their ease of separation using an appropriate external magnetic field. The emergence of rGO with Ag NPs as hybridized nanocomposites produces promising compounds with improving performance and enhancing the photodegradation, biological, antimicrobial, and anti-bacterial effects [23]. This work seeks to generate rGO@Ag hybrid NPs using a simple and environmentally safe approach to improve the photodegradation of CR dye from an aqueous solution. Furthermore, to show the factors affecting the photocatalytic processes.

A facile and eco-friendly method to synthesis rGO@Ag NPs was carried out to degrade Congo red dye from aqueous solution. This study is organized in several sections, Sect. 2 shows the experimental sequences of preparation and characterization rGO@Ag NPs and demonstrate the main factors affecting the CR degradation. Section 3 represents the detailed characterization of as-syntheses NPs and discussed the main factors affecting degradation process. The next two Sects. 4 & 5 emphasizing the obtained results using different adsorption and kinetic models. Finally, Sect. 6 provides the conclusion.

2 Materials and methods

All chemicals contain; graphite powered (99.9%), sulfuric acid (H_2SO_4 98%), CR dye ($C_{32}H_{24}N_6O_6S_2.2Na$, λmax = 497 nm), silver nitrate NPs ($AgNO_3$), H_2O_2 (30%), $KMnO_4$, HCl (36%), acetone, and absolute ethanol are Sigma–Aldrich grade.

2.1 Synthesis of graphene oxide (GO)

Graphene oxide NPs were synthesized using modified Hummer's method. Briefly, 5 g of graphite NPs were added to conc. H_2SO_4 (98%, 60 mL) in an ice container, 2.5 g of $NaNO_3$ was additionally add with continuous magnetic stir for 40 min; after that, 15 g of $KMnO_4$ slowly added with vigorous magnetic stir overnight. After that, carefully adding a suitable amount of deionized distilled water, 40 ml of H_2O_2 (30%) was added dropwise with continuous stirring for 40 min, the temperature raised gradually up to 50 °C. The produced precipitate was washed multiple times with HCl (4%) and deionized distilled water. Centrifugation of the mixture at 8000 rpm for 7 min was carried out to precipitate the residue and dried it at 80 °C.

2.2 Preparation of rGO@Ag NPs

Synthesis of rGO@Ag NPs was produced by merging $AgNO_3$ with GO. 10 g of GO was suspended in 500 mL DW and sonicated for 2 h. $AgNO_3$ (0.1 M) solution was added in a different amount to the GO mixture to obtain; 2%,4%, 6% rGO@Ag NPs. Solution of NaOH (0.1 M) was used to adjust solution pH to ~ 10. The mixture was re-sonicated for 20 min after adding 10% lactulose solution.

2.3 Characterizations of rGO@Ag NPs

Mettler-Toledo V670 USA, spectroscopy was used to determine the effect of variation Ag NPs ratio on the prepared nanocomposites between 250 and 800 nm. In addition, the energy gap (Eg) for several nanocomposites was estimated using UV–Visible spectroscopy results. XRD pattern was used to assess the crystalline features of prepared NPs using X-ray diffractometer (Model PW-3710). XRD was operated with Cu-Kα radiation ($\lambda = 1.5418$ Å) in the range of $2\theta = 10°$–$80°$ with the rate of scan $2\theta = 5°$/min. At 200 kV acceleration voltage, the emission scanning electron microscope (Carl Zeiss, America) was employed to analyze the morphology of as-synthesized rGO@Ag nanocomposites (SEM, TEM). The elemental compositions of the catalyst were determined by EDX spectroscopy. Different functional groups on the surface of as-prepared catalysts were discovered using FT-IR "Fourier transform infrared spectroscopy" spectrum technology (6700 FTIR, Nicolet, USA) in the 4000–400 cm^{-1} range.

2.4 Photocatalytic study

1000 mg/L solution of CR dye was prepared. Afterthat, standard solutions with various concentrations were prepared as needed. The photocatalytic degradation experiments were done under UV light (6 mercury lamps of 11 Watt were used). The irradiation wavelength was set to be less than 300 nm. Several major parameters were investigated to evaluate the removal effectiveness of as-synthesized photocatalysts, including solution pH, contact duration, catalyst dosages, and initial concentration of CR dye. The sorption–desorption equilibrium was attained with stirring the mixtures at 350 rpm/min with the photocatalysts in the dark for 30 min. This stage was repeated for each researched factor under different experimental conditions. Solutions' pH ranging between 4 and 10 was selected to study the pH effect through 100 ml CR dye (50 mg/L). Also, the effect of contact time (15–120 min), catalysts dosages (0.05–0.5 g/L), and Initial dye concentration (0.5–50 mg/L) were investigated to indicate the optimum removal conditions. An aliquot (5 ml) from each mixture was centrifuged at 7000 rpm for 7 min, and the supernatant concentration was measured at $\lambda = 497$ nm using Jenway 6800UV/VIS spectrophotometer. Photocatalytic efficiency (q_e) was calculated according to Eq. 1;

$$q_e = \frac{(C_0 - C_e) \times V}{M},$$ (1)

where V is the volume of solution (L), C_0 initial CR concentration, Ce concentration of CR at equilibrium, and M is catalyst mass (g).

3 Results and discussion

3.1 Characterization

Figure 1 shows the UV–Vis spectra for as-synthesized photocatalysts with wavelengths ranging from 200 to 700 nm (1). An obvious peak at 245 nm belongs to rGo NPs, and this band arises mainly from τηπε-π* transition of the C=C bond [24]. Three peaks were detected with a slight shift to higher wavelength to 255, 260, and 270 nm belonging to 2%, 4, and 6% rGo@Ag NPs, respectively. Also, these bands belong to $\pi - \pi*$ transitions [25]. This shift indicated that the Ag NPs were impregnated with decreased graphene. These findings are similar to those of [26], who observed maximum peaks ranging from 253 to 265 nm for rGO and rGO/Ag NPs synthesis. Furthermore, Abdalla et al. [23]

Fig. 1 UV—VIS spectra of as-synthesis rGO and rGO@Ag$_x$ nanoparticles
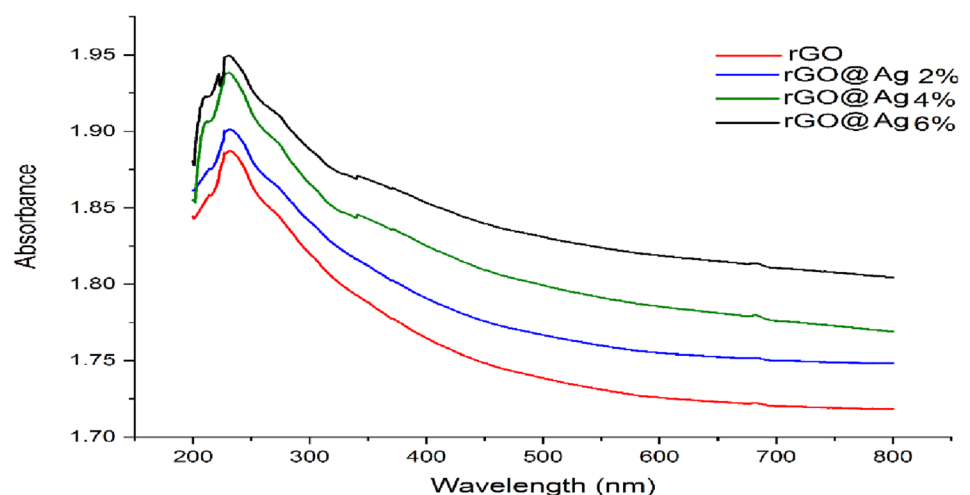
observed a peak at 230 nm for belonging to C–C bonds and a strong peak at ~ 440 nm of Ag/rGO.

Using the Tauc equation, data from UV–Vis absorption of as-synthetic nanoparticles were utilized to compute the bandgap energy (Eg) for each nanocomposite. A graph between $(\alpha h\nu)^2$ against hv was plotted (Fig. 2). The interception of the tangent of the curve with the X-axis represented the E_g value. The estimated Egs from the curves are; 2.41, 2.26, 2.18, and 2.08 eV for rGO and rGO@Ag 2%, 4%, and 6% NPs respectively. Significant decrease in computed energy gap (Eg) with increasing the doping Ag % with rGO NPs, indicating an improvement in photocatalytic efficiency.

Figure 3 denotes the crystallographic and phase composition of the prepared nanoparticles using XRD analyses; the XRD data resemble the standard JCPDS card NO 00-004-0783. The XRD pattern of rGO nanocomposites exhibits two crystalline peaks at 2 = 14.32° and 42.72° with d-spacing of 7.81 and 2.11 corresponding to the (002) and (031). These two peaks disappeared in the XRD pattern

of rGO@Ag x% due to Ag NPs anchoring on the surface of rGO NPs leading to the prevention of stacking of rGO particles [27]. Javed et al. [28] reported that several peaks at 38.07, 44.28, 64.50 were belonging to Ag with (111), (200), (220) planes which confirm the amorphous crystal shape phases of rGo NPs. Another six peaks appeared in the XRD pattern of rGO@Ag x% NPs at 2θ = 32.45° (110), 38.31° (111), 46.52° (200), 64.53° (220), 78.5° (311), and 82.67 (222), which indicated the cubic crystalline planes of the Ag NPs phase (JCPDS No. 04-0783). Some literatures proved that the synthesized Ag/rGO nanocomposite can improve its efficiency due to Ag NPs and increase the adsorption of dye molecules due to presence of rGO [29]. Furthermore, Wu et al. [30] reported a dense peak for rGO at 24.3∘

The SEM images were used to identify morphological characteristics and determine the distribution and particle size of as-synthesized nanoparticles (Fig. 4). Furthermore, the elemental composition was determined using EDX analysis (Fig. 5). SEM images of rGO NPs clarified
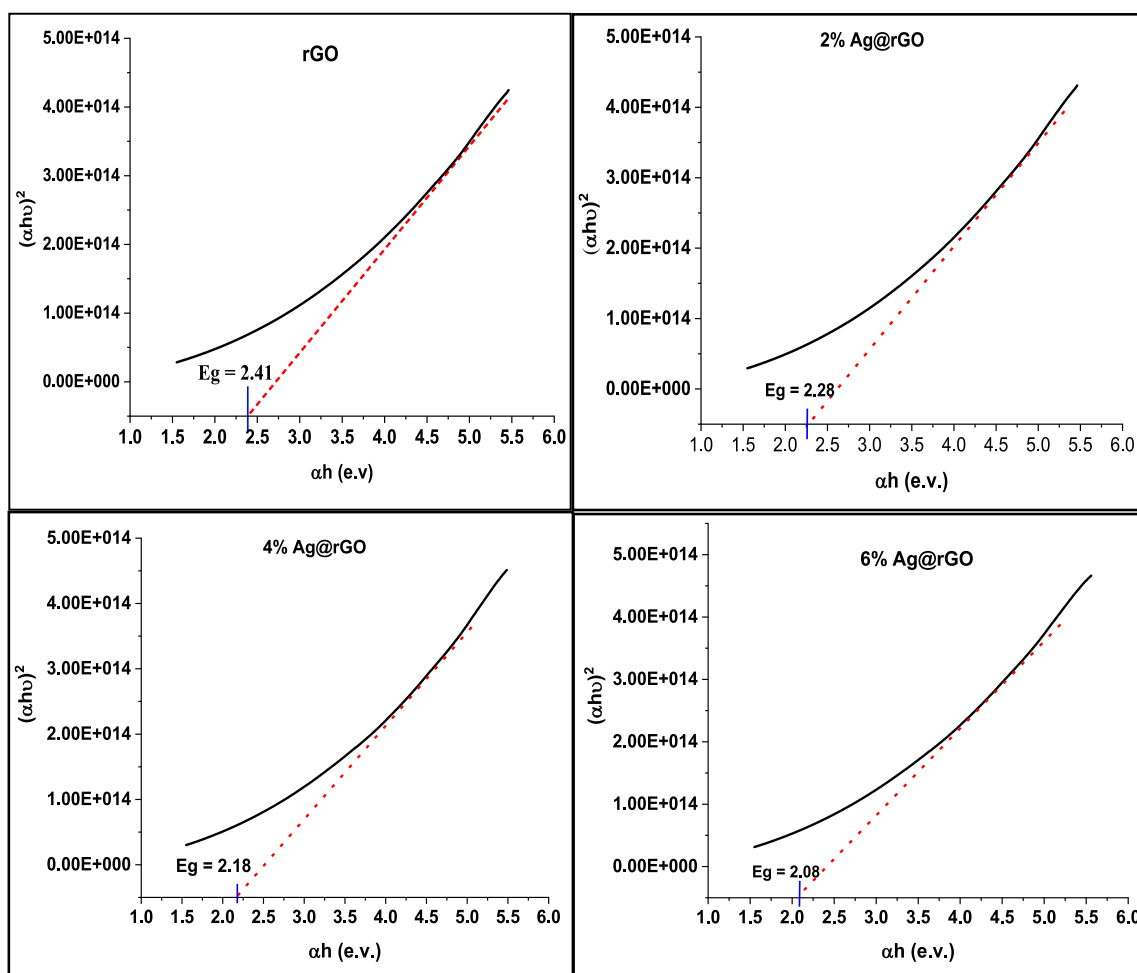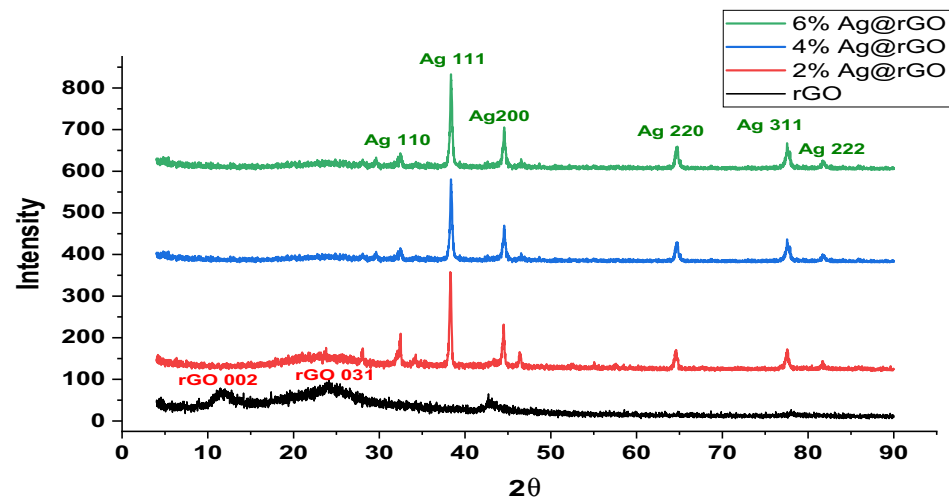

Fig. 2 Tauc's plot of for estimation the energy band gap (Eg) of the prepared photocatalysts

Fig. 3 XRD Spectra of rGO, rGO@Ag 2%, rGO@Ag 4% and rGO@Ag 6% nanocomposite

homogeneous lamellar surface with highly porous and deep grooves of the surface of rGO nanocomposites (Fig. 4a), the particle sizes ranging from 19.45 to 24.84 nm (Fig. 4b). An imbedded silver NPs were observed as visible brilliant dots on the surface of rGO@Ag x% NPs (Fig. 4c and d) declaring stuck of Ag NPs onto the surface of rGO [31, 32] Maham et al. [31], Hasija et al. [32]. However, Rahman et al. [33] showed similar particle size $Ag_2O@La_2O_3$ nanosheets ranged between 7.5 and 14.7 nm. While Dippong et al. [34] reported that, $Cu_xCo_{1-x}Fe_2O_4/$ SiO_2 nanocomposites (NCs) with high Cu content have 40–70 nm but with high Co content have smaller grain sized (15–25 nm).

In the EDX spectrum picture of manufactured rGO NPs, two main peaks were visible; the first peak belonged to carbon (40.25%) and oxygen (36.85%), and another two minor peaks Cl (15.55%) and K (7.35%) (Fig. 4a). However, in rGO@Ag x percent NPs, a significant silver (11.2%) peak developed alongside the peaks of carbon and oxygen with ratios of 55.2% and 32.6%, respectively (Fig. 4b).
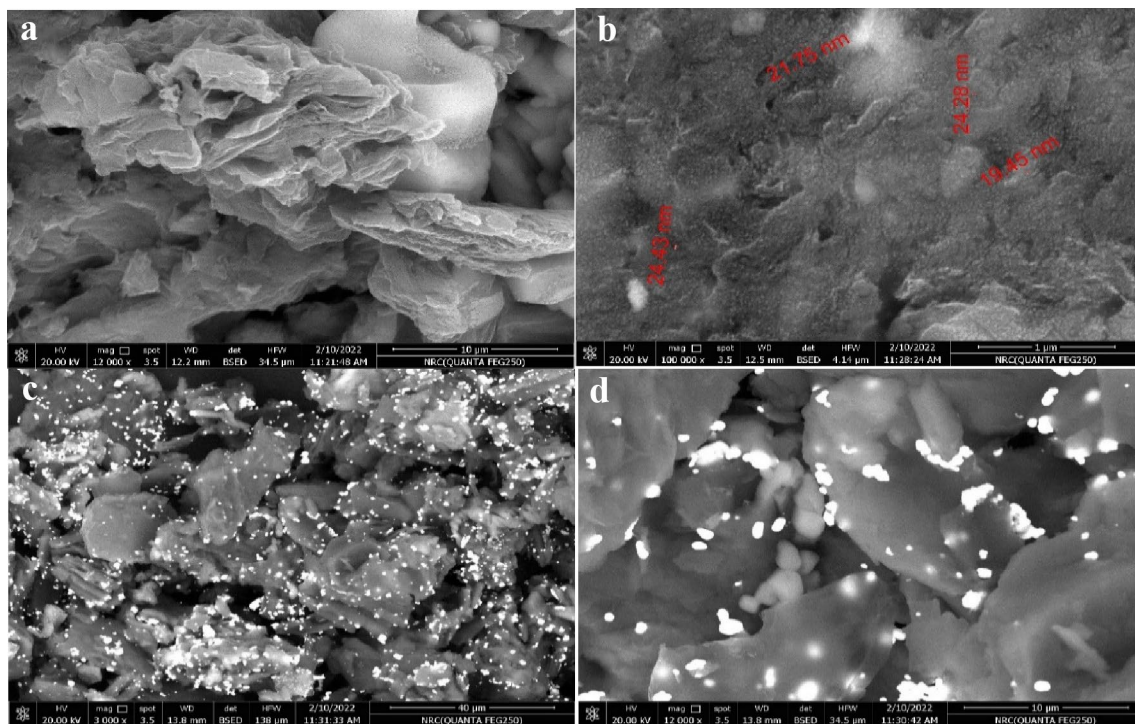

Fig. 4 SEM images of (a) rGO, (b) rGO@Ag 2%, (c) rGO@Ag 4% and (d) rGO@Ag 6% nanocomposite
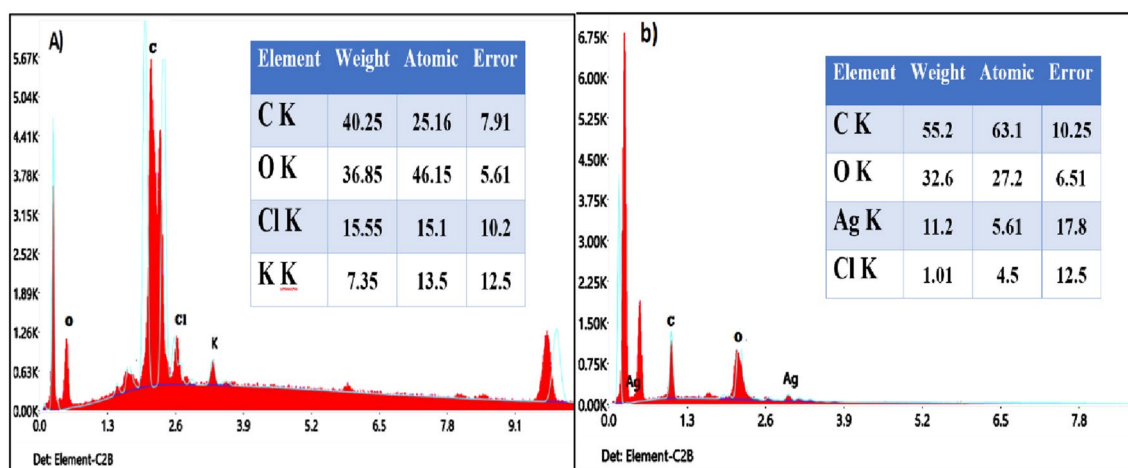
Fig.5 EDX analysis spectra of **a** rGO, and **b** rGO@Ag x % nanocomposites

A transmission electron micrograph (TEM) was carried out to detect the particle size and agglomeration. TEM images showed non agglomerated, spherical shape of rGO NPs with scattered silver particles adhered to rGO particles (Fig. 6). The particle size of as-synthesized NPs was ranged between 17.36 and 25.97 nm (rGO NPs) and 8.54–10.28 nm (rGO/Ag NPs). These results revealed that the prepared nanoparticles have low size distribution range about at 22 and 10 nm for rGO and rGO/Ag with nearly aggregated particles [35].

T-IR technique was used to detect the functional groups synthesized catalyst. (Figure. 7) shows the FT-IR spectrum bands ranged between 4000 and 400 cm^{-1}. A significant wide peak was observed at 3431 cm^{-1} (93.2%), which belong to stretching hydroxyl group (O–H) in water [36]. Another two bands occurred at 2923 and 2304 cm^{-1}, which corresponding to =C–H vibration stretching and acid O–H group [32]. Weak two peaks were observed at 1663 and 1349 cm^{-1} belonging to amide C=O and epoxy C-O groups [37]. A low intensity peak was appeared at 1119 cm^{-1} which attributed to –C–O and C–O–H stretching vibrations of alcohols [38]. Smaller peak was detected at 796–650 cm^{-1}, which belong to Ag-halide stretching, proving the formation of rGO@Ag x% nanoparticles [32]. These results may be due to the interaction between the functional groups which containing oxygen in rGO NPs with Ag NPs [39].

3.2 Photocatalytic activities

3.2.1 Effect of pH

The solution's pH plays a highly important role in the photodegradation of different dyes and organic compounds [40] . The impact of varied pH degrees on the photodegradation of CR was investigated using solutions with pH ranging from 4 to 10 with an initial CR content of 50 mg/L and 0.4 g/L photocatalysts (Fig. 8). To reach sorption–desorption equilibrium, the mixtures were stirred at 350 rpm in dark place for 30 min. Then after, the solutions are exposed to UV-irradiation for 120 min. The highest degradation efficiency (q_e) of the rGO catalyst was 78.4 mg/g and rose marginally with increasing Ag doping ratio, reaching 82.22, 83.28, and 89.06 mg/g for rGO@Ag 2%, 4%, and 6%, respectively was achieved at pH 7. Mahapatra et al. [41] and Cheng et al. [42] reported maximum degradation of CR dye at pH 7 using γ-Fe_2O_3-Al_2O_3 and Al-Fe_2O_3/LDH NPs (Table 1).

The generation of ·OH free-radical at pH > 7 (lower than pH_{ZPC} of CR dye) enhances the breakdown of CR molecules. Furthermore, the obvious decrease in the photocatalytic process at higher pH values > 9 is attributed to the negatively charged surface of the catalyst due to hydroxyl group aggregation in the solution. Thus, an electrostatic repulsion force was formed between the negatively charged CR molecules and the negatively surfaces of photocatalysts [7, 9].

3.2.2 Effect of time

The effect of UV irradiation contact time was conducted between 15 and 150 min to detect the maximum degradation efficiency of 50 mg/L initial concentration of CR using 0.4 5/L photocatalysts at pH = 7 (Fig. 9). With increasing the contact irradiation time, obvious photodegradation progress of CR was detected, reaching around 62 percent, after which a slowdown of the reaction was observed until it reached the maximum photodegradation efficiency after 120 min, after which
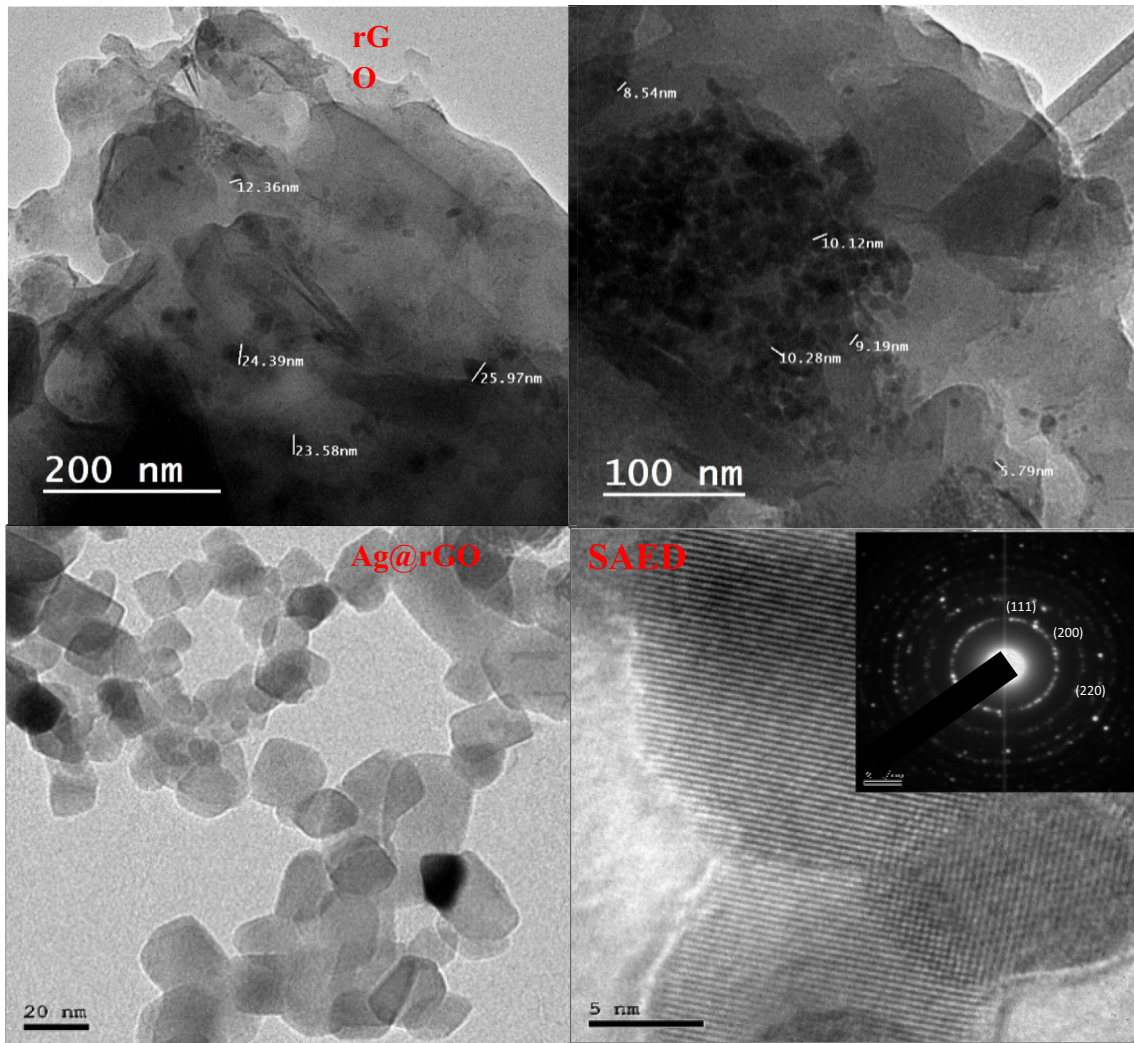
Fig. 6 Transmission electron microscope (TEM) and SAED images of as-synthesized rGO, rGO@Ag x% nanocomposites

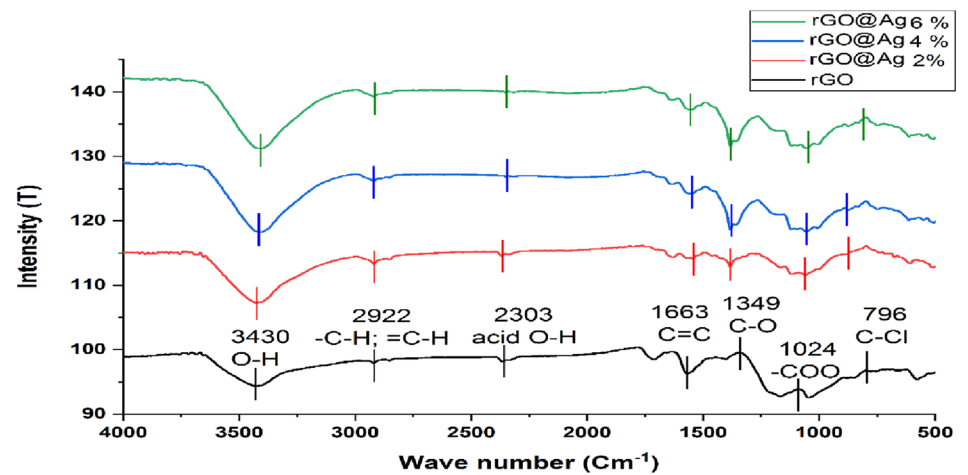**Fig. 7** FT-IR of rGO, rGO@Ag 2%, rGO@Ag 4% and rGO@Ag 6% NPs

Fig. 8 Effect of solution pH on the photodegradation efficiency of Congo red dye under optimum conditions
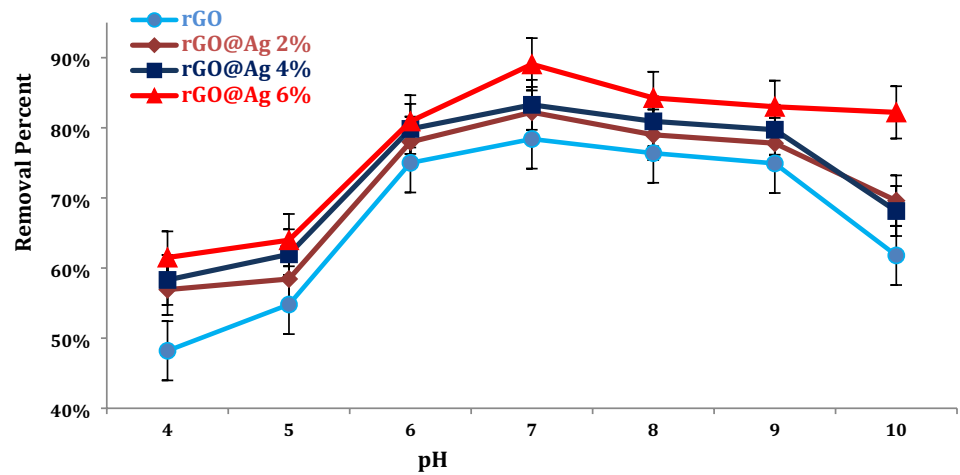

Table 1 Comparison between degradation of different organic dyes using different photocatalysts

Organic substrate	Catalyst	pH	Time (min)	Dose (g/L)	Eff. mg/g	Ref
Amaranth	CoFeNPs1	6	53	0.67	11	[46]
Acid orange	(CoFeNPs2)	60	150	0.67	9	[46]
Congo red	γ-Fe$_2$O$_3$-Al$_2$O$_3$	7	15	0.1	498	[41]
Congo red	Al-Fe$_2$O$_3$/LDH	5.5	30	0.005	1364	[42]
Methylene orange	ZnO	6.0	50	0.3	90	[47]
Methylene blue	Ag$_2$S@Ag	*	5	0.075	99.83	[43]
Congo red	ZnO@Ze	3	20	0.05	161	[48]
Rhodamine B	Ag–Cu@ZnO	*	0.2	0.05	99	[44]
Methylene blue	CdS/SnO$_2$ NPs	*	180	0.1	90	[49]
methylene orange	SnO$_2$-SnS$_2$	*	60	0.05	99	[50]
Congo red	ZnO@Ze	3	20	0.05	99.5%	[43]
Congo red	Ag–Cu@ZnO	*	15	0.005	90%	[44]
Congo red	Fe$_3$O$_4$/SiO$_2$/ZnO/Pr$_6$O$_{11}$	*	80	0.02	84.7%	[51]
Congo red	rGo, Ag@rGO	7	120	0.4	89	Recent data

*not available

Fig. 9 Photodegradation of Congo red dye under different contact time interval
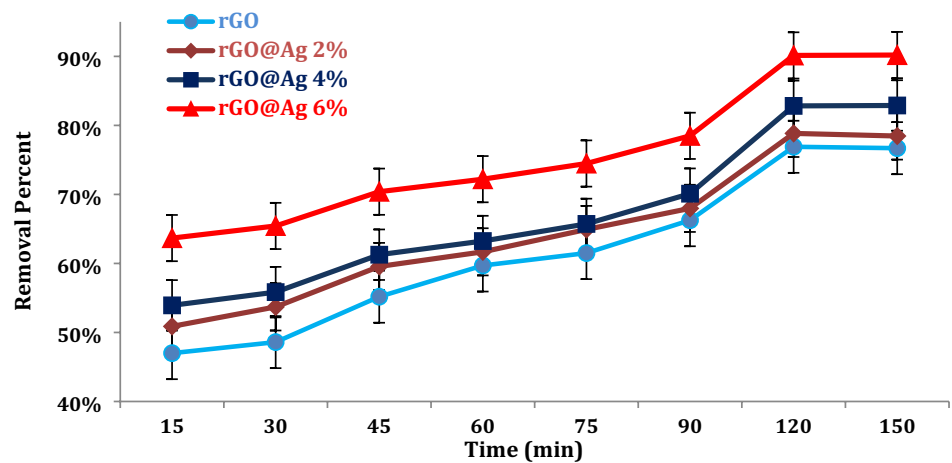
the reaction was steady until it reached equilibrium. rGO catalyst has the lowest degradation efficiency ($q_e = 76.9$ mg/g); by increasing the Ag doping ratio, a remarkable increase of Qe was achieved; 78.84, 82.8, and 90.2 mg/g for rGO@Ag 2%, 4%, and 6% respectively. Several researches [7, 40, 43, 44] found that maximum degradation of CR dye was achieved at 90, 105, 20 and 15 min different photocatalysts (Table 1).

3.2.3 Effect of dose

Different quantities of the prepared photocatalysts NPs (0.05 to 0.5 g/L) were used to determine the optimum catalyst dose required for the maximum degradation of CR dye (50 mg/L CR concentration) with pH = 7 during 120 min as contact time. Figure 10. depicts the steady increase of CR dye photodegradation with increasing catalyst dosages, with maximum removal precents of 85.8, 87.8, 86.8, and 88.6 for rGO, and rGO@Ag 2%, 4%, and 6%, respectively, at 0.4 g/L catalyst quantity. When the quantity of photocatalyst is increased, the photodegradation rate decreases, which is related to the

aggregation of photocatalyst particles, lowering the photocatalytic activity of the catalyst. Al-Onazi and Ali [7] reported 0.3 g/L of CeO@chitosan NPs for maximum CR degradation.

3.2.4 Initial dye concentration effect

Figure 11 represents the removal percent of CR with different concentrations (5 to 50 mg/L). Using 0.4g/l photocatalysts at pH 7 and 120 min contact time. Although there was an evident negative association between the removal % and the CR dye starting concentration for all utilized as-synthesized catalysts, raising the CR dye concentration enhanced photodegradation efficiencies (q_e). Low CR dye concentrations degrade fast due to the high surface area availability of the employed catalysts and low formation intermediates that compete with original CR molecules [45]. With the increase of the CR concentrations, the removal percent was lowered, but the q_e increased to reach maximum values of 79.0, 81.2, 83.3, and 84.4 mg/g for rGO, rGO@Ag 2%, 4%, and 6%, respectively.

Fig. 10 Photodegradation of Congo red dye using different photocatalyst doses
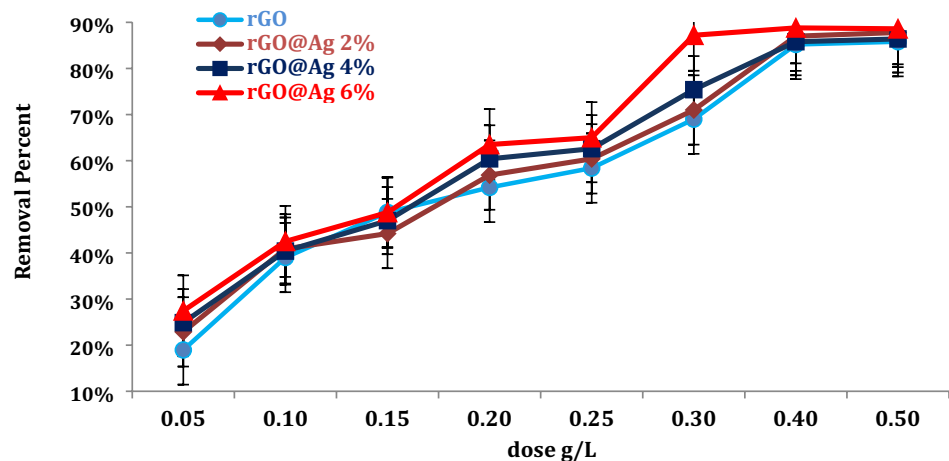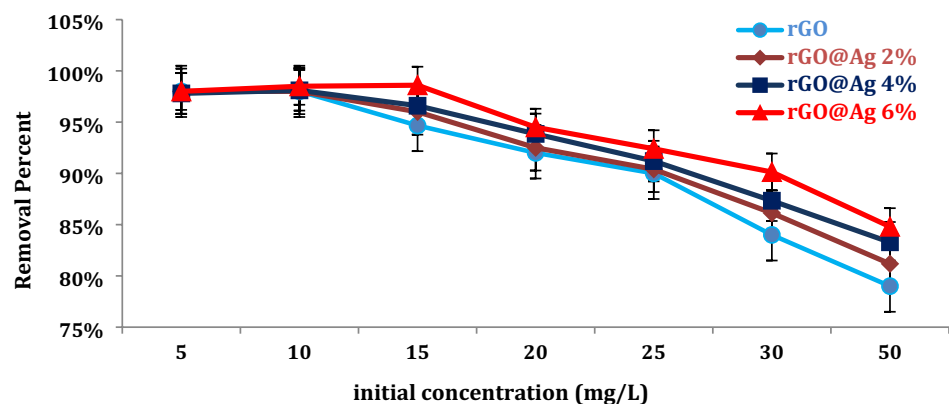

Fig. 11 Photodegradation of Congo red dye using different initial concentration of CR dye

4 Isothermal studies

Langmuir and Freundlich isothermal models were used to explore degradation suitability. The Langmuir isotherm model predicts the occurrence of homogeneous adsorption with maximal adsorption capacity (q_{max}) and Langmuir constant (b), which means the affinity of the adsorption. Freundlich suggests a multilayer heterogeneous adsorption process. Both Langmuir and Freundlich models are calculated in the following eqs (Eq. 2 & Eq. 3):

$$\text{Langmuir Equation } q_e = \frac{q_{max}bc_e}{1 + bC_e}, \tag{2}$$

$$\text{Freundlich equation } q_e = K_f C_e^{\frac{1}{n}} \tag{3}$$

where: q_{max} (mg^{-1}) is the maximum uptake of adsorbate; b Langmuir constant ($L.mg^{-1}$), q_e ($mg.g^{-1}$) is the amount of absorbed substrate; C_e (gL^{-1}) the absorbed substrate concentration at equilibrium; K_f is the absorbent capacity and n is the adsorption intencity.

The results obtained from Langmuir and Freundlich isothermal models showed insignificant difference indicating that, the two models accurately represent the degradation of CR dye with R^2 almost > 0.95 (Table 1 & Figs. 12 and 13). Furthermore, the calculated R_L constant (dimensionless constant) was ranged between 0.0009 and 0.012 indicating favorable adsorption of CR dye according to classification of McKay et al. [52] reported that, if R_L values ranged between $0 < R_L < 1$, thus a favorable adsorption type is occurred (Table 2). These findings are consistent with those of Al-Onazi and Ali [7] for the CR dye photodegradation using ceria NPs. Furthermore, Guo et al. [6] demonstrated that the CR dye degradation followed the Langmuir and Freundlich models when NiS NPs were used.

5 Kinetics studies

Kinetics models are valuable tools for predicting the contaminant removal rate from aqueous solutions. Two typical kinetic models, pseudo-first order and pseudo-second order models, are used to explore the adsorption process of CR dye onto as-synthesized NPs. The two models were expressed linearly as in (Eq. 4) and (Eq. 5) as the following;

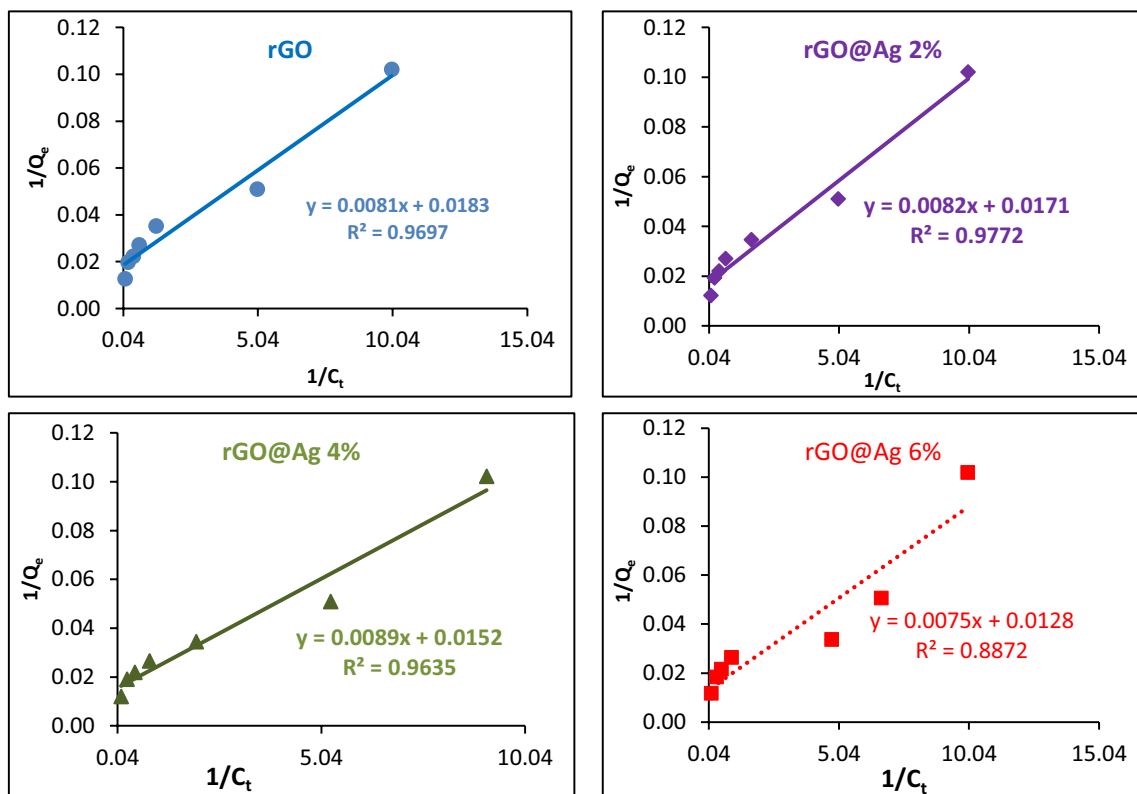$$\log\left(C_e - C_t\right) = \log C_e - \frac{k_1}{0.203}t, \tag{4}$$

Fig. 12 Graph of Langmuir isotherm model for CR degradation using as-synthesized rGO and rGO@Ag x % nanocomposites
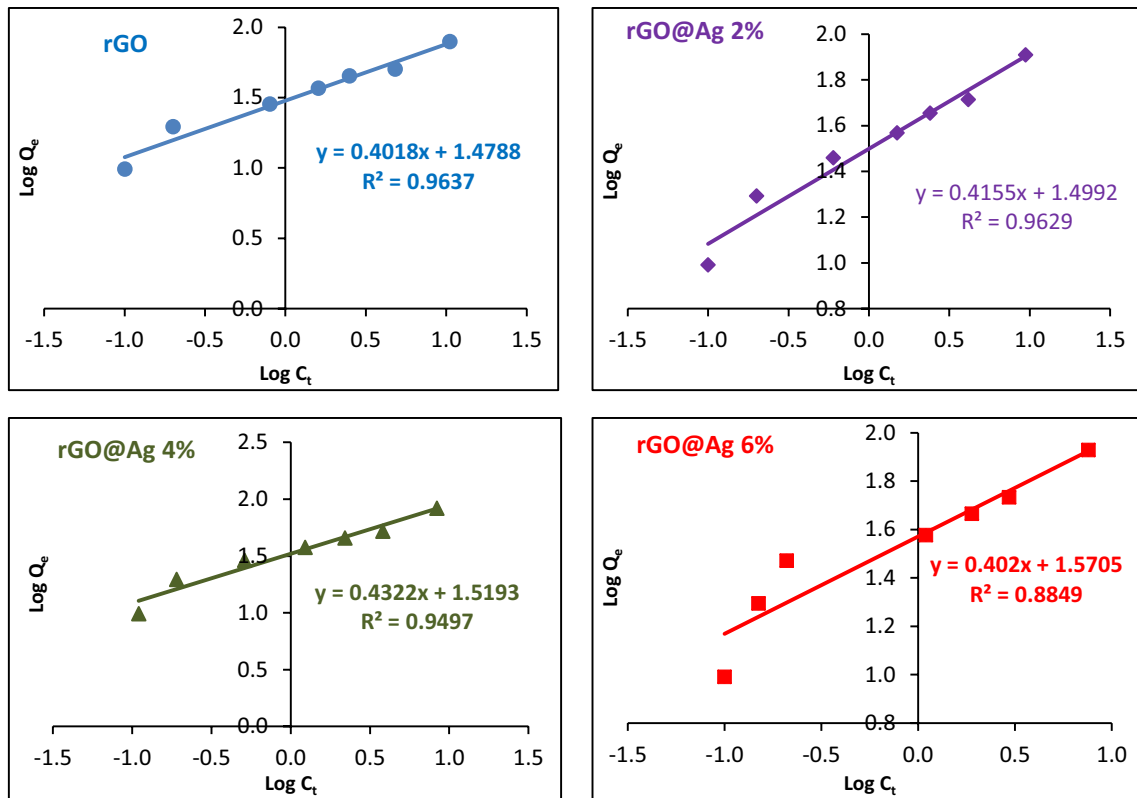
Fig. 13 Graph of Freundlich isotherm model for CR degradation using as-synthesized rGO and rGO@Ag x % nanocomposites

Table 2 Constants of Langmuir and Freundlich models for the degradation of CR dye

Catalyst	Langmuir isotherm				Freundlich isotherm		
	b	q_{max}	R_L	R^2	K_f	n	R^2
rGO	2.26	54.64	0.009	0.97	30.12	2.49	0.96
rGO@Ag 2%	2.09	58.48	0.010	0.98	31.56	2.41	0.96
rGO@Ag 2%	1.71	65.79	0.012	0.96	33.06	2.31	0.95
rGO@Ag 2%	1.71	78.13	0.012	0.89	37.20	2.49	0.89

$$\frac{t}{C_t} = \frac{1}{k_2 C_e^2} + \frac{1}{C_e}t, \qquad (5)$$

Figures 14 and 15 showed the linear curve of the two kinetic models. The calculated kinetic constants are given in Table 2. The low correlation coefficient (R^2) obtained for the pseudo-first order model (mainly < 0.78) with corresponding low Q_e values (< 0.6 mg/L) is regarded as not ideal for exploring the CR adsorption mechanism and indicates that these experimental data did not obey the pseudo-first order kinetic reaction. Contrarily, the linear relation between t/Q_t versus t (Fig. 14) showed high correlation coefficients (R^2 are nearly close to 1) with high Q_e values ranging between 86.95 − 98.04 mg/g (Table 3). These findings demonstrated
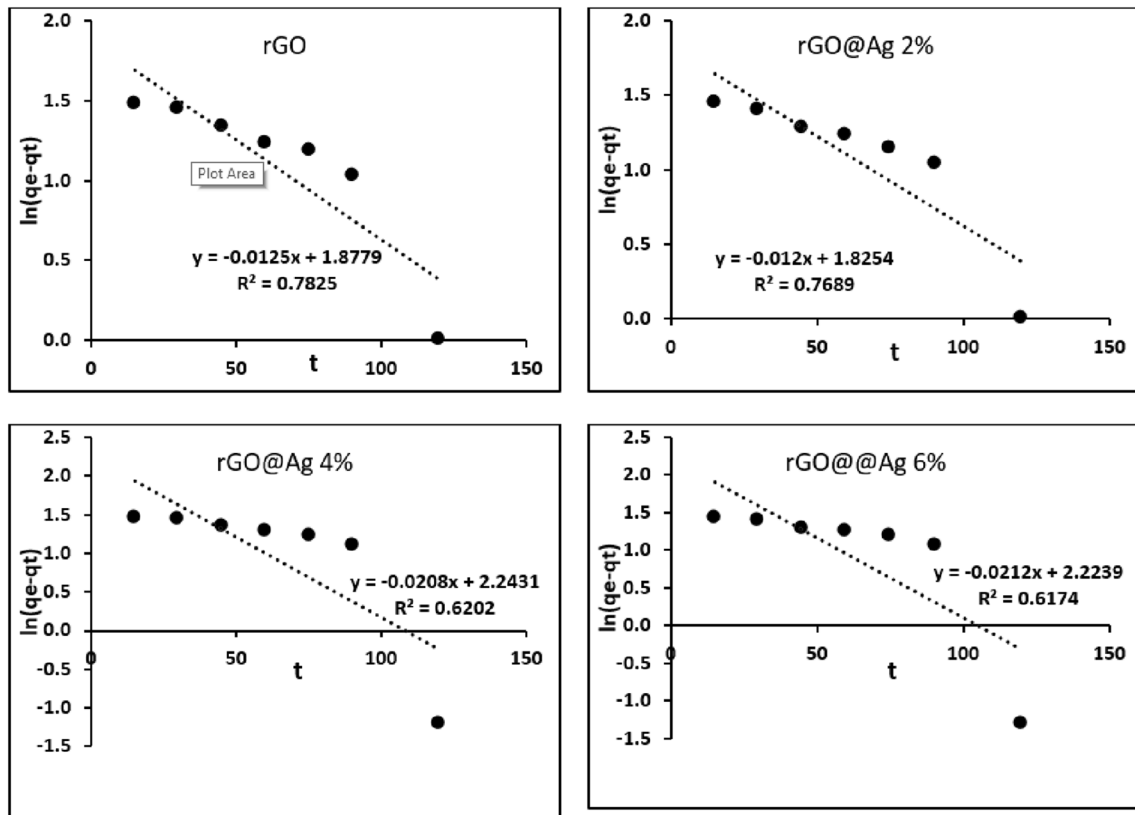
Fig. 14 Graph of the pseudo-first-order reaction for CR dye degradation using as-synthesized rGO and rGO@Ag x nanocomposites

that the CR dye adsorption kinetics onto as-synthesized NPs optimally matched the pseudo-second order reaction.

6 Conclusion

In this study a simple and eco-friendly environmental method was employed to synthesize rGO and rGO@Ag NPs. The photocatalyst was characterized physically to investigate the morphology, optical characteristics, elemental composition, particle size distribution and the existence functional groups using SEM, EDX, TEM, UV–VIS, XRD and FT-IR investigations. These investigations declared successful stuck of Ag NPs on the rGO surface. The average particle sizes ranging from 17.36–25.97 to 8.54–10.28 nm for rGO and rGO/Ag NPs respectively. A low energy gaps of 2.41, 2.26, 2.18, and 2.08 eV were estimated for rGO, and rGO@Ag 2%, 4% and 6% NPs respectively. The as-synthesized photocatalyst nanoparticle was used for enhancing the degradation of CR dye degradation under UV irradiation. The photodegradation experiment showed that pH = 7 was optimum for the maximum degradation process, with maximum degradation efficiency (q_e) reaching 89 mg/g at 120 min and 0.4 g/L catalyst dosage, initial concentration 50 mg/L of CR dye and 120 min contact time. The isothermal studies revealed that the isotherm models of Langmuir and Freundlich accurately represent CR dye photodegradation, with R^2 almost > 0.95. kinetically, the pseudo-second order reaction model was more express the adsorption process with Q_e values ranging between 86.95 and 98.04 mg/L and corresponding R^2 of > 0.99. The results proved that Ag doping of rGO enhances its effective photocatalytic performance.
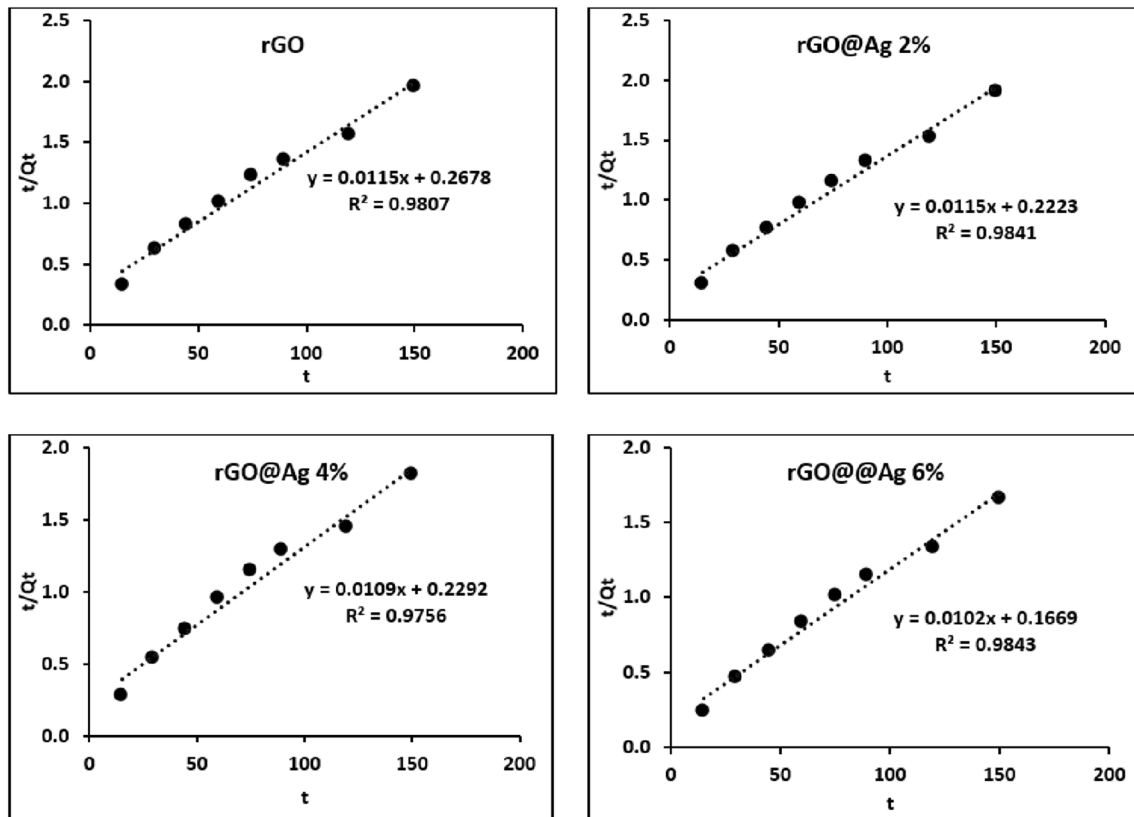
Fig. 15 Graph of the pseudo-second-order reaction for CR dye degradation using as-synthesized rGO and rGO@Ag x nanocomposites

Table 3 The calculated constants of pseudo-first and pseudo-second order reactions for CR dye degradation using rGO and rGO@Ag nanocomposites

Catalyst	Pseudo-first order reaction			Pseudo-second order reaction		
	Q_e	K_1	R^2	Q_e	K_2	R^2
rGO	0.533	2.88E-02	0.7825	86.95	4.94E-04	0.9807
rGO@Ag 2%	0.548	4.79E-02	0.7689	86.95	5.95E-04	0.9841
rGO@Ag 4%	0.446	4.79E-02	0.6202	91.74	5.18E-04	0.9756
rGO@Ag 6%	0.450	4.88E-02	0.6174	98.04	6.23E-04	0.9843

Declarations

References

1. Ali MH, Al-Qahtani KM, El-Sayed SM (2019) Enhancing photo-degradation of 2,4,6 trichlorophenol and organic pollutants in industrial effluents using nanocomposite of TiO_2 doped with reduced graphene oxide. Egypt J Aquatic Res 45(4):321–328. https://doi.org/10.1016/j.ejar.2019.08.003

2. Islam A, Teo SH, Taufiq-Yap YH, Ng CH, Vo DVN, Ibrahim ML, Awual MR (2021) Step towards the sustainable toxic dyes removal and recycling from aqueous solution - A comprehensive review. Resour Conserv Recycl 175:105849. https://doi.org/10.1016/j.resconrec.2021.105849

3. Teo SH, Ng CH, Islam A, Abdulkareem-Alsultan G, Joseph CG, Janaun J, Awual MR (2021) Sustainable toxic dyes removal with advanced materials for clean water production: a comprehensive review. J Clean Prod. https://doi.org/10.1016/j.jclepro.2021.130039

4. Ali MH, Goher ME, Al-Afify DG (2019) Kinetics and adsorption isotherm studies of methylene blue photodegradation under UV irradiation using reduced graphene oxide-TiO_2 nanocomposite in different wastewaters effluents. Egypt J Aquatic Biol Fisheries 23(1):253–263

5. Nadjia L, Abdelkader E, Ahmed B (2011) Photodegradation study of Congo Red in aqueous solution using ZnO/UV-A: Effect of pH and band gap of other semiconductor groups. J Chem Eng Process Technol 2(2):1–9. https://doi.org/10.4172/2157-7048.1000108

6. Guo H, Ke Y, Wang D, Lin K, Shen R, Chen J, Weng W (2013) Efficient adsorption and photocatalytic degradation of Congo red onto hydrothermally synthesized NiS nanoparticles. J Nanopart Res 15(3):1–12. https://doi.org/10.1007/s11051-013-1475-y

7. Al-Onazi WA, Ali MH (2021) Synthesis and characterization of cerium oxide hybrid with chitosan nanoparticles for enhancing the photodegradation of Congo Red dye. J Mater Sci 32(9):12017–12030. https://doi.org/10.1007/s10854-021-05832-7

8. Afkhami A, Moosavi R (2010) Adsorptive removal of Congo red, a carcinogenic textile dye, from aqueous solutions by maghemite nanoparticles. J Hazard Mater 174(1–3):398–403. https://doi.org/10.1016/j.jhazmat.2009.09.066

9. Bhat SA, Zafar F, Mondal AH, Kareem A, Mirza AU, Khan S, Nishat N (2020) Photocatalytic degradation of carcinogenic Congo red dye in aqueous solution, antioxidant activity and bactericidal effect of NiO nanoparticles. J Iran Chem Soc 17(1):215–227. https://doi.org/10.1007/s13738-019-01767-3

10. Znad H, Abbas K, Hena S, Awual MR (2018) Synthesis a novel multilamellar mesoporous TiO_2/ZSM-5 for photo-catalytic degradation of methyl orange dye in aqueous media. J Environ Chem Eng 6(1):218–227. https://doi.org/10.1016/j.jece.2017.11.077

11. Alam MM, Asiri AM, Uddin MT, Islam MA, Awual MR, Rahman MM (2019) Detection of uric acid based on doped ZnO/Ag_2O/Co_3O_4 nanoparticle loaded glassy carbon electrode. New J Chem 43(22):8651–8659. https://doi.org/10.1039/C9NJ01287G

12. Yeamin MB, Islam MM, Chowdhury AN, Awual MR (2021) Efficient encapsulation of toxic dyes from wastewater using several biodegradable natural polymers and their composites. J Clean Prod 291:125920. https://doi.org/10.1016/j.jclepro.2021.125920

13. Awual MR (2019) Efficient phosphate removal from water for controlling eutrophication using novel composite adsorbent. J Clean Prod 228:1311–1319. https://doi.org/10.1016/j.jclepro.2019.04.325

14. Chowdhury MF, Khandaker S, Sarker F, Islam A, Rahman MT, Awual MR (2020) Current treatment technologies and mechanisms for removal of indigo carmine dyes from wastewater: a review. J Mol Liq 318:114061. https://doi.org/10.1016/j.molliq.2020.114061

15. Rani M, Yadav J, Shanker U (2020) Efficient degradation of nonylphenol and 2, 4-dinitrophenol by sunlight responsive hexacyanocobaltates nanostructures. Environ Nanotechnol Monit Manag 14:100325. https://doi.org/10.1016/j.enmm.2020.100325

16. Rajendran S, Hoang TK, Trudeau ML, Jalil AA, Naushad M, Awual MR (2022) Generation of novel npn (CeO_2-PPy-ZnO) heterojunction for photocatalytic degradation of micro-organic pollutants. Environ Pollut 292:118375. https://doi.org/10.1016/j.envpol.2021.118375

17. Naushad M, Alqadami AA, Al-Kahtani AA, Ahamad T, Awual MR, Tatarchuk T (2019) Adsorption of textile dye using para-aminobenzoic acid modified activated carbon: kinetic and equilibrium studies. J Mol Liq 296:112075. https://doi.org/10.1016/j.molliq.2019.112075

18. Aboutaleb WA, El-Salamony R (2019) Effect of Fe_2O_3-CeO_2 nanocomposite synthesis method on the Congo red dye photodegradation under visible light irradiation. Mater Chem Phys 236:121724. https://doi.org/10.1016/j.matchemphys.2019.121724

19. Thomas M, Naikoo GA, Sheikh MUD, Bano M, Khan F (2016) Effective photocatalytic degradation of Congo red dye using alginate/carboxymethyl cellulose/TiO2 nanocomposite hydrogel under direct sunlight irradiation. J Photochem Photobiol, A 327:33–43. https://doi.org/10.1016/j.jphotochem.2016.05.005

20. Elaziouti LN, Ahmed B (2011) ZnO-Assisted photocatalytic degradation of congo red and benzopurpurine 4B in aqueous solution. J Chem Eng Process Technol 2:106. https://doi.org/10.4172/2157-7048.1000106

21. Kumar A, Kaur H (2020) Sprayed in-situ synthesis of polyvinyl alcohol/chitosan loaded silver nanocomposite hydrogel for improved antibacterial effects. IInt J Biol Macromol 145:950–964. https://doi.org/10.1016/j.ijbiomac.2019.09.186

22. Ali MH, Al-Afify AD, Goher ME (2018) Preparation and characterization of graphene–TiO_2 nanocomposite for enhanced photodegradation of Rhodamine-B dye. The Egypt J Aquatic Res 44(4):263–270. https://doi.org/10.1016/j.ejar.2018.11.009

23. Abdalla JT, Wang J, Wang D (2019) Effect of Ag/rGO on the optical properties of plasmon-modified SnO_2 composite and its application in self-powered UV photodetector. Curr Comput-Aided Drug Des 9(12):648. https://doi.org/10.3390/cryst9120648

24. Wu T, Liu S, Luo Y, Lu W, Wang L, Sun X (2011) Surface plasmon resonance-induced visible light photocatalytic reduction of graphene oxide: using Ag nanoparticles as a plasmonic photocatalyst. Nanoscale 3(5):2142–2144. https://doi.org/10.1039/c1nr10128e

25. Huang J, Zong C, Shen H, Ca Y, Ren B, Zhang Z (2013) Tracking the intracellular drug release from graphene oxide using surface-enhanced Raman spectroscopy. Nanoscale 5(21):10591–10598. https://doi.org/10.1039/C3NR03264G

26. Pusty M, Rana AK, Kumar Y, Sathe V, Sen S, Shirage P (2016) Synthesis of partially reduced graphene oxide/silver nanocomposite and its inhibitive action on pathogenic fungi grown under ambient conditions. ChemistrySelect 1(14):4235–4245. https://doi.org/10.1002/slct.201600783

27. Mott D, Thuy NTB, Aoki Y, Maenosono S (2010) Aqueous synthesis and characterization of Ag and Ag-Au nanoparticles: addressing challenges in size, mono dispersity and structure. Philos Trans R Soc A Math Phys Eng Sci 368:4275–4292. https://doi.org/10.1098/rsta.2010.0120

28. Javed HMA, Qureshi AA, Mustafa MS, Que W, Mahr MS, Shaheen A, Mahmood A (2019) Advanced Ag/rGO/TiO2 ternary nanocomposite based photoanode approaches to highly-efficient plasmonic dye-sensitized solar cells. Optics Commun 453:124408. https://doi.org/10.1016/j.optcom.2019.124408

29. Shah MS, Muhammad S, Park JH, Yoon WS, Yoo PJ (2015) Incorporation of PEDOT: PSS into SnO_2/reduced graphene oxide nanocomposite anodes for lithium-ion batteries to achieve ultra-high capacity and cyclic stability. RSC Adv 5(18):13964–13971. https://doi.org/10.1039/C4RA15913F

30. Wu J, Lan Z, Lin J, Huang M, Huang Y, Fan L, Wei Y (2017) Counter electrodes in dye-sensitized solar cells. Chem Soc Rev 46(19):5975–6023. https://doi.org/10.1039/C6CS00752J

31. Maham M, Nasrollahzadeh M, Sajadi SM, Nekoei M (2017) Biosynthesis of Ag/reduced graphene oxide/Fe3O4 using Lotus garcinii leaf extract and its application as a recyclable nanocatalyst for the reduction of 4-nitrophenol and organic dyes. J Colloid Interface Sci 497:33–42. https://doi.org/10.1016/j.jcis.2017.02.064

32. Hasija V, Sudhaik A, Raizada P, Hosseini-Bandegharaei A, Singh P (2019) Carbon quantum dots supported AgI/ZnO/phosphorus doped graphitic carbon nitride as Z-scheme photocatalyst for efficient photodegradation of 2,4-dinitrophenol. J Environ Chem Eng 7(4):103272. https://doi.org/10.1016/j.jece.2019.103272

33. Rahman MM, Sheikh TA, Asiri AM, Awual MR (2019) Development of 3-methoxyaniline sensor probe based on thin Ag_2O@ La_2O_3 nanosheets for environmental safety. New J Chem 43(11):4620–4632. https://doi.org/10.1039/C9NJ00415G

34. Dippong T, Levei EA, Lengauer CL, Daniel A, Toloman D, Cadar O (2020) Investigation of thermal, structural, morphological and photocatalytic properties of $Cu_xCo_{1-x}Fe_2O_4$ (0≤ x≤ 1) nanoparticles embedded in SiO_2 matrix. Mater Charact 163:110268. https://doi.org/10.1016/j.matchar.2020.110268

35. Dippong T, Toloman D, Levei EA, Cadar O, Mesaros A (2018) A possible formation mechanism and photocatalytic properties of CoFe2O4/PVA-SiO2 nanocomposites. Thermochim Acta 666:103–115. https://doi.org/10.1016/j.tca.2018.05.021

36. Soleymani AR, Rafigh SM, Hekmati M (2020) Green synthesis of RGO/Ag: As evidence for the production of uniform mono-dispersed nanospheres using microfluidization. Appl Surf Sci 518:146264. https://doi.org/10.1016/j.apsusc.2020.146264

37. Botsa SM, Basavaiah K (2019) Removal of Nitrophenols from wastewater by monoclinic CuO/RGO nanocomposite. Nanotechnol Environ Eng 4(1):1–7. https://doi.org/10.1007/s41204-018-0045-z

38. Rafigh SM, Heydarinasab A (2017) Hydroxyethyl curdlan as a novel water soluble derivative: synthesis, characterization, and antioxidant capacity. Int J Polym Anal Charact 22(6):497–508. https://doi.org/10.1080/1023666X.2017.1331390

39. Wadhwa H, Kumar D, Mahendia S, Kumar S (2017) Microwave assisted facile synthesis of reduced graphene oxide-silver (RGO-Ag) nanocomposite and their application as active SERS substrate. Mater Chem Phys 194:274–282. https://doi.org/10.1016/j.matchemphys.2017.03.045

40. Ouyang J, Zhao Z, Suib SL, Yang H (2019) Degradation of Congo Red dye by a Fe2O3@ CeO2-ZrO2/Palygorskite composite catalyst: synergetic effects of Fe_2O_3. J Colloid Interface Sci 539:135–145. https://doi.org/10.1016/j.jcis.2018.12.052

41. Mahapatra A, Mishra BG, Hota G (2013) Adsorptive removal of Congo red dye from wastewater by mixed iron oxide–alumina nanocomposites. Ceram Int 39(5):5443–5451. https://doi.org/10.1016/j.ceramint.2012.12.052

42. Cheng S, Shao L, Ma J, Xia X, Liu Y, Yang Z, Li S (2019) Simultaneous removal of phosphates and dyes by Al-doped iron oxide decorated MgAl layered double hydroxide nanoflakes. Environ Sci Nano 6(8):2615–2625. https://doi.org/10.1039/C9EN00520J

43. Madan S, Patel SR, Rahgozar K, Saeed O, Murthy S, Vukelic S, Jorde UP (2019) Utilization rates and clinical outcomes of hepatitis C positive donor hearts in the contemporary era. J Heart Lung Transplant 38(9):907–917. https://doi.org/10.1016/j.healun.2019.06.023

44. Manjari G, Saran S, Radhakrishanan S, Rameshkumar P, Pandikumar A, Devipriya SP (2020) Facile green synthesis of Ag–Cu decorated ZnO nanocomposite for effective removal of toxic organic compounds and an efficient detection of nitrite ions. J Environ Manag 262:110282. https://doi.org/10.1016/j.jenvman.2020.110282

45. MirzaHedayat B, Noorisepehr M, Dehghanifard E, Esrafili A, Norozi R (2018) Evaluation of photocatalytic degradation of 2,4-Dinitrophenol from synthetic wastewater using Fe_3O_4@SiO_2/TiO_2/rGO magnetic nanoparticles. J Mol Liq 264:571–578. https://doi.org/10.1016/j.molliq.2018.05.102

46. Qurrat-Ul-Ain KS, Gul Z, Khatoon J, Shah MR, Hamid I, Khan IAT, Aslam F (2020) Anionic azo dyes removal from water using amine-functionalized cobalt–iron oxide nanoparticles: a comparative time-dependent study and structural optimization towards the removal mechanism. RSC Adv 10(2):1021–1041. https://doi.org/10.1039/C9RA07686G

47. Zafar MN, Dar Q, Nawaz F, Zafar MN, Iqbal M, Nazar MF (2019) Effective adsorptive removal of azo dyes over spherical ZnO nanoparticles. J Market Res 8(1):713–725. https://doi.org/10.1016/j.jmrt.2018.06.002

48. Zhang H, Chen M, Wang D, Xu L, Liu X (2016) Laser induced fabrication of mono-dispersed Ag_2S@ Ag nano-particles and their superior adsorption performance for dye removal. Optic Mater Exp 6(8):2573–2583. https://doi.org/10.1364/OME.6.002573

49. El-Katori EE, Ahmed MA, El-Bindary AA, Oraby AM (2020) Impact of CdS/SnO_2 heterostructured nanoparticle as visible light active photocatalyst for the removal methylene blue dye. J Photochem Photobiol, A 392:112403. https://doi.org/10.1016/j.jphotochem.2020.112403

50. Yadav S, Asthana A, Chakraborty R, Jain B, Singh AK, Carabineiro SA, Susan MABH (2020) Cationic dye removal using novel magnetic/activated charcoal/β-cyclodextrin/alginate polymer nanocomposite. Nanomaterials 10(1):170. https://doi.org/10.3390/nano10010170

51. Ebrahimzadeh MA, Mortazavi-Derazkola S, Zazouli MA (2020) Eco-friendly green synthesis of novel magnetic Fe3O4/SiO2/ZnO-Pr6O11 nanocomposites for photocatalytic degradation of organic pollutant. J Rare Earths 38(1):13–20. https://doi.org/10.1016/j.jre.2019.07.004

52. McKay G, Blair HS, Gardner JR (1982) Adsorption of dyes on chitin. I. Equilibrium studies. J Appl Polym Sci 27(8):3043–3057. https://doi.org/10.1002/app.1982.070270827